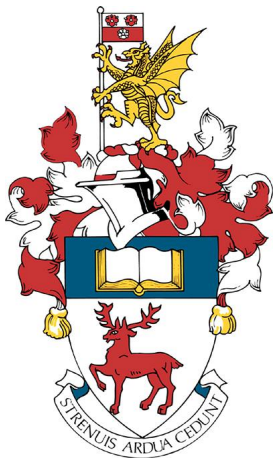

THE UNIVERSITY OF SOUTHAMPTON

FACULTY OF ENGINEERING & THE ENVIRONMENT

GROUP DESIGN PROJECT

Development of a Hydrofoiling Experimental Research Platform

Mandles Prize

Authors:
A. Ayan, Univeristy of Southampton, UK, asenaayan1@gmail.com
T. Ballantine, Univeristy of Southampton, UK, tomballantine@live.co.uk
J. Carson, Univeristy of Southampton, UK, jeromecarson@msn.com
J. Diamond, Univeristy of Southampton, UK, jamiediamond@me.com
F. Hayes, Univeristy of Southampton, UK, fredhayes21@yahoo.com
S. Jones, Univeristy of Southampton, UK, samakj@live.co.uk
A. Vose, Univeristy of Southampton, UK, annabel@upstartventures.co.uk

Supervisors:
S.W. Boyd, Univeristy of Southampton, UK, S.W.Boyd@soton.ac.uk

May 2017

Abstract

Interest in hydrofoil technology is rapidly growing within the marine industry due to development classes such as the International Moth and in the America's Cup. There is large potential for analysis and development in the use of foils to reduce drag and enhance the performance of high speed sailing vessels. This has lead to the creation of a research platform with the aim of creating an interface in which the experimental testing of innovative hydrofoil technology can be effectively carried out.

This report outlines the design and manufacture process of creating a Nacra F18 foiling test platform, using J shaped main foils and T shaped rudders. A pod system was developed to attach the foils to the side of the boat and the rudders were designed to have interchangeable elevators, allowing for different combinations of main foils and rudder elevators to be investigated. These are the two main features that affect the forces acting on the boat and are therefore very important when developing a foiling boat. The boat's response to real world conditions were analysed through the collection of performance data such as velocities, accelerations, wind speeds and angles. A velocity prediction program to model non-foiling and foiling sailing performance was designed to provide a basis for performance prediction and comparison with experimental data. This program has been refined using data from computational fluid dynamics analysis of hydrofoils and compared using the data gathered from towing and sailing testing.

The test platform was successfully developed to allow a F18 catamaran to foil without the need for hull modifications. Design and manufacture were achieved within a short time frame, under a strict budget, involving a variety of analytical, computational and experimental methods. The systems have all been tested in strong wind conditions and proved to be robust and structurally reliable. Data acquisition has allowed for video footage to be compared with quantitative data to improve the understanding of the platforms performance and behaviour. The development of a foiling velocity prediction program has been used throughout the project to ascertain boat speeds for lift calculations and ensuring the efficiency of test days. The program predicts take-off speeds which were validated by ultrasound results from testing. The combination of the foiling platform, data acquisition and velocity prediction will allow future research into developing foiling technologies.

NOMENCLATURE AND ABBREVIATIONS

Symbol	Definition	[unit]
A	Area	$[m^2]$
α	Rake Angle	[°]
AoA	Angle of Attack	[°]
AWA	Apparent Wind Angle	[°]
AWS	Apparent Wind Speed	$[Knots]$
C_D	Drag Coefficient	
CFD	Computational Fluid Dynamics	
C_L	Lift Coefficient	
CNC	Computer Numerically Controlled	
DAQ	Data Acquisition	
F_x	Drive Force	$[N]$
F_y	Side Force	$[N]$
F_z	Lift Force	$[N]$
GFRP	Glass Fibre Reinforced Plastic	
GPIO	General Purpose Input and Output	
IMU	Inertial Measurement Unit	
JSON	Java Script Object Notation	
λ	Leeway Angle	[°]
ORC	Offshore Racing Congress	
ρ	Density	$[kgm^{-3}]$
$_{rh}$	Ride Height	$[m]$
RPi	Raspberry Pi	
$_s$	Board Strut	
$_t$	Board Tip	
TWA	True Wind Angle	[°]
TWS	True Wind Speed	$[Knots]$
θ	Cant Angle	[°]
UDP	User Datagram Protocol	
VNC	Virtual Network Computing	
VPP	Velocity Prediction Program	
V_S	Boat Speed	$[m/s]$
x	Vertical Distance	$[m]$
Z_{ce}	Centre of Effort	$[m]$

1 INTRODUCTION

The development of hydro-foiling catamarans, during the 34th America's Cup cycle, has bought hydro-foiling to the attention of the general sailing community, with several other classes now adopting the technology. Considerable research is being undertaken at the America's Cup level however this is not publicly accessible. The project aim was therefore to produce a platform to allow similar research to be undertaken at an undergraduate level.

A Nacra F18 is an 18 foot racing catamaran built to the F18 class rules [1]. The boat was designed before the introduc-

tion of lifting foils to racing catamarans, so features straight dagger-boards. A set of Nacra F20 FCS main foils were made available at the start of the project, however the design and manufacture of T-foil rudders and a system to attach the foils to the hull was required.

A VPP was developed to predict the performance of the platform by balancing aero and hydrodynamic forces. A data acquisition system was installed to record experimental results for comparison to and validation of the VPP.

2 BACKGROUND

2.1 RUDDERS

Hydrofoiling craft require lifting surfaces on the rudders to provide pitch control and subsequently flight stability. A new set of rudders was designed for the platform consisting of two components; the strut and an elevator. Both components are solid pre-preg carbon fibre laminate, manufactured using aluminium female moulds. The rudders were deliberately overbuilt to ensure a robust system. Utilising the freedom and flexibility that arrived with the decision of building the rudders completely from scratch and inspired by the potential for future research of this experimental platform, the rudders were designed to allow for interchangeable elevators. This would then allow different elevators to be attached to the strut with relative ease, providing an area for future hydrofoil research. Different elevator design factors such as aspect ratio, area, foil section and AoA could be explored. Both 2D foil section and 3D CFD analyses were carried out using Xfoil and Star CCM+ v. 11 throughout rudder design and optimisation.

2.2 PODS

The project aims were to develop a system to retro-fit hydrofoils to the F18 without making any major modifications to the hull. As such, a system to attach the hydrofoils to the F18 was developed. This had to be capable of transferring the large loads developed by the foils to platform, as well as allowing adjustment to the foil configuration. This included the development of systems to raise and lower the boards, as well a rake control system to adjust the angle of attack and hence lift generated by the foils.

2.3 DATA ACQUISITION SYSTEM

In the development of a 'research platform' it is of primary importance that the relevant platform and environment metrics can be measured. In this case the areas of interest were as follows: wind speed/heading, platform speed/heading and platform dynamics, these were chosen as key metrics area in order to be able to analyse the stability and effect of changes on the dynamics of foiling.

3 RUDDERS

3.1 DESIGN CONSIDERATIONS

Based on research from existing T-foil rudders it was decided that the strut would be tapered. This would provide sufficient area at the top to fit the stock and reduce wetted area and hence skin friction when foiling whilst still maintaining good control at low speeds. It would also reduce weight and material requirements. The design therefore starts with a larger cross section at the top and ends with a smaller section at the tip. The horizontal lift-generating wing would be placed at the tip, as done in the Nacra and Moth rudders. The wing was also to have a taper, with a large cross section in the middle to allow for a structurally strong and stable attachment to the strut. Utilising the freedom and flexibility associated with the decision of building the rudders completely from scratch, and inspired by the potential for future research of this experimental platform, it was decided that the rudders would allow for interchangeable tips. This would then allow different elevators to be attached to the strut with relative ease, providing an area for future hydrofoil research. Different elevator design factors such as aspect ratio, area, foil section and AoA could be explored.

3.2 2D FOIL SECTION ANALYSIS

The cross sectional shape of hydrofoils is an extremely important design consideration as it directly affects the lift and drag characteristics. It was decided that 4-Digit NACA foils were to be used for both the strut and elevator cross sections due to their simple generation and availability of extensive research and data.

In order to determine which sections to utilise in the T-foil rudder strut and elevator, a study on five 2D NACA foil sections was carried out using XFOIL. The chosen sections were generated using NACA foil formulas. Symmetrical foils were preferred as it was assumed that the T-foil rudder would be required to provide lift in both directions when sailing. As the elevator to strut attachment was an important factor to consider throughout the design process, the 2D foils that were tested were chosen to have sufficient thickness for various forms of structural connection. The flow was calculated to have a Reynolds number in the order of 1×10^6 which indicates the flow is likely to be turbulent. The lift and drag characteristics of each foil at varying AoA in the range $0 - 7^\circ$ were obtained and plotted against the ratio of lift and drag coefficients, C_L and C_D, in order to gain a better understanding of foil performance, Figure 1.

It can be seen that the NACA0006 section performs with the highest lift for a given drag at angles of attack up to 2°, after which the performance begins to depreciate as stalling occurs. The other thin sections, 0008 and 0009, also perform in a similar manner, but the stalling angle occurs at higher angles of attack; performance at higher angles begins to improve the thicker the section becomes. The NACA0012 and 0015 sections perform the most consistently throughout the range of angles, with 0012 resulting in slightly higher C_L/C_D values. Based on these results, it was decided that the elevator would consist of a NACA0012 section at its midspan as it provided good performance characteristics over a wider range of angles of attack and was thought to be thick enough to house internal structure for connection with the strut.

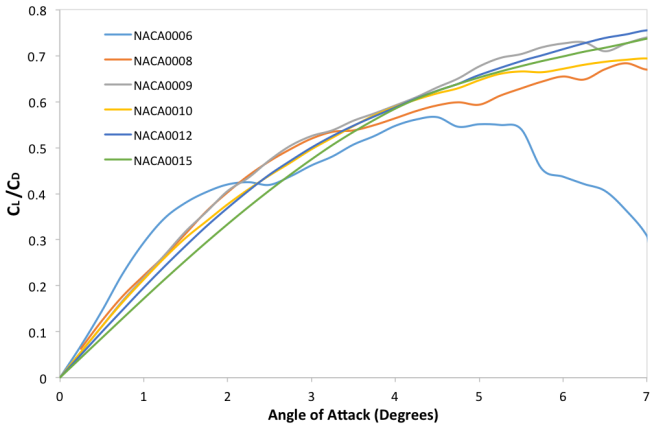

Figure 1: Lift and drag coefficient ratio vs. angle of attack of 2D NACA foil sections.

3.3 3D ANALYSIS

Having carried out 2D foil analysis, the rudders were analysed as a 3D problem using CFD, and so a 3D model of the rudder was created. Several main factors including the size of the elevator, the position at which the strut intercepted the elevator and the thickness of the bottom section of the strut were investigated by creating and testing a range of models with varying geometry.

3.3.1 MESH

A structured mesh was utilised for the 3D CFD testing of the various rudder and elevator geometries. As there were many configurations to test, a new mesh was required for each model, thus computational time required to obtain an adequate mesh was a key primary issue before results were able to be obtained. In order to combat this, a structured mesh was preferred due to faster and easier generation, lower data storage requirements and better convergence rates. The boundary layer was refined with a finer mesh of 15 layers to capture smaller details of the flow.

3.3.2 SOLVERS AND BOUNDARY CONDITIONS

The analysis was set up using the following solvers: steady state, liquid, segregated flow, constant density, turbulent, and K-Omega turbulence models. These solvers were believed to represent the physical flow around the rudder adequately. The liquid was set to have properties of seawater at $15°C$, with a constant input density of $1026kgm^{-3}$ and dynamic viscosity of $1.23\times10^{-}3kgm^{-1}s^{-1}$. Boundary conditions were applied to allow for one infinitely large wall with a slip condition, one symmetrical plane through the rudder's centreline, and a non-slip condition on the foil surface to capture the surface's effects on forces.

3.3.3 RESULTS

The first phase of CFD analysis investigated elevator dimensions placed in constant position relative to the strut, which was made to have a generic NACA0012 shape and taper based on preliminary dimensions. Five different elevators were designed and the lift to drag ratios were obtained to provide a comprehensive comparison of the effect of varying geometry on elevator performance, seen in Figure 2. The elevator with dimensions $150 \times 80 \times 500mm$ (Case 4) was determined to be the best case as it produced a large enough lifting surface and performed well throughout all angles of attack. Its hight aspect ratio was also an advantage due to the reduced tip vortices.

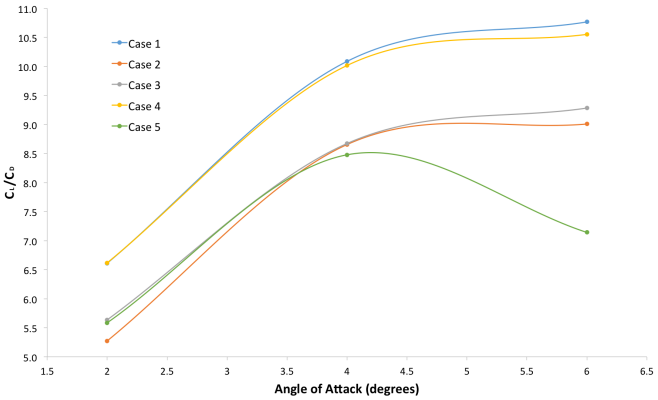

Figure 2: Lift to drag ratio of tested elevator dimensions.

The second phase of CFD analysis investigated the effect of elevator attachment position on the strut and changing strut dimensions on overall rudder performance. Cases 1 and 2 assess the difference between having the elevator set forwards on the strut or set aft. Case 3 was used to explore the effect of increasing the NACA section of the strut from 0012 to 0016. Figure 3 shows that Strut Case 1, or placing the elevator aligned aft on the strut, produced the best C_L/C_D ratio for the range of AoA. This was supported by a wake flow analysis shown in Figures 4 and 5; there is reduced recirculation and thus drag in this strut case. The optimum geometry of the rudder is given in Table 1.

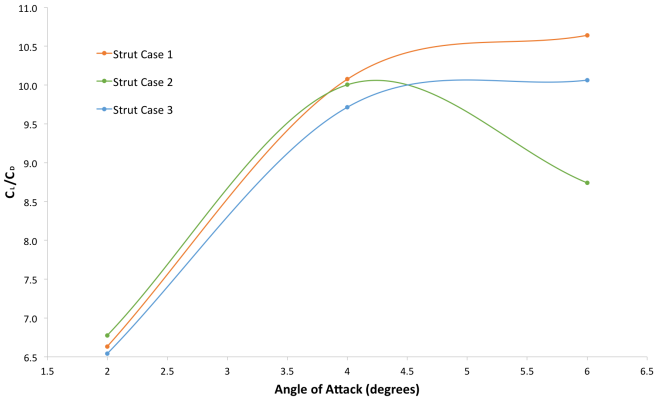

Figure 3: Lift to drag ratio of tested elevator strut orientations.

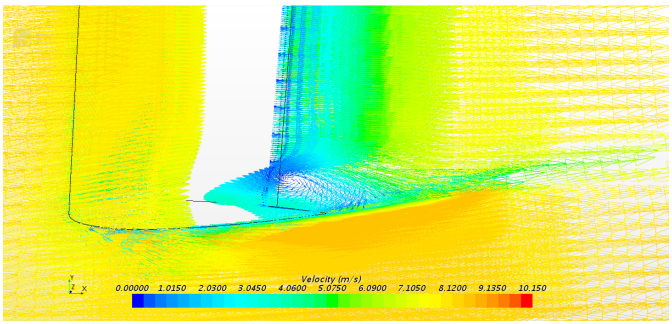

Figure 4: Flow at cross section of strut with elevator forward.

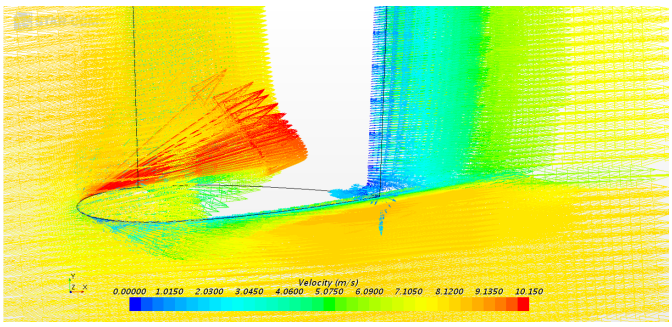

Figure 5: Flow at cross section of strut with elevator aft.

3.4 MANUFACTURE

The rudders were manufactured from solid pre-preg carbon fibre using aluminium female moulds. This was to ensure that the rudders would be robust enough to withstand multiple use, as the platform was intended to enable future research. This also allowed us to develop a system by which the elevators could be changed with ease to allow multiple different elevators to be used in a single testing session. This system involved embedding a Stainless Steel T-section into the bottom of the strut that would then allow the elevator to be bolted onto the strut. This can be seen in Figure 6 which shows the bottom section of the rudder.

4 PODS

4.1 FOILS

Professionally manufactured Nacra F20 FCS foils were used for the project as the university facilities were not geared up for the manufacture of composite components of this scale. These types of foils are commonly referred to as J-foils, which are composed of two sections; a strut and a tip. The effective cant of the foil means the configuration acts as a surface piercing foil, which provides a degree of passive heave control. The Nacra F20 FCS has a combined boat and crew weight of approximately 70kg less than the modified F18, so the foils are slightly too small for the application. The F20 is significantly wider and has a larger sail area, so is capable of applying more power, therefore take-off wind speed is likely to be significantly higher for the modified F18.

Table 1: Rudder final dimensions.

Strut	
NACA Section	0012
Top Chord $[mm]$	200
Bottom Chord $[mm]$	120
Length $[m]$	1.5
Elevator	
NACA Section	$0012 \rightarrow 0004$
Central Chord $[mm]$	150
Tip Chord $[mm]$	80
Width $[m]$	0.5

Figure 6: Elevator attachment for the rudder.

4.2 FOIL ATTACHMENT SYSTEM

The project brief stated that no major modifications were to be made to the hull. To achieve this, a removable system for mounting the hydro-foils was developed. This was composed of a GFRP cradle which wrapped half way around the hull, and a aluminium frame to support the foil bearings. The frame was attached to the cradle using Bighead fasteners; a type of stainless steel fastener with a large, flat head designed to be embedded in composite structures. To ensure an adequate load path, the foil attachment system was positioned at the existing daggerboard case. This provided a reinforced area to transfer the loads to the hull, while also providing a hole through the depth of the hull to clamp the system in place. From a boat dynamics viewpoint, this position also places the centre of lateral resistance in the correct place. However, from a pitching moment perspective the foil position is further aft than is optimal, as the driving force is limited by the extent to which the crew can move their weight aft.

Attaching the foils using this system, as shown in Figure 7, helps to increase the available righting moment of the vessel by increasing the distance from the centreline to the centre of lift. The cradle also has a negative impact on the flow field around the hull, the effect of which could be reduced with the addition of fairings.

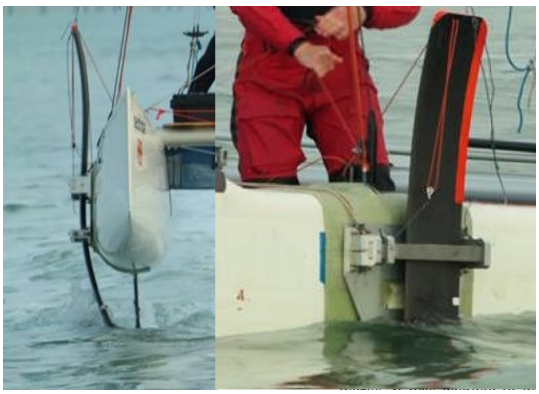

Figure 7: Front and side view of pod attachment system and lifting foils.

4.3 FRAME DESIGN

A finite element model was created to analyses the strength of the aluminium frame. The forces applied to the system were generated using conservative free-body diagrams which were used to predict the maximum moments generated by the foils, as shown in Figure 8. A screen shot of the FEA analysis is shown in Figure 9, with this design feaaturing a safety factor of 1.7.

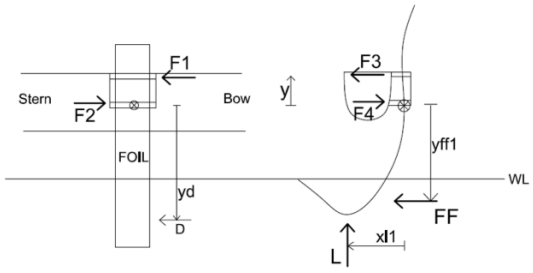

Figure 8: Conservative free-body diagram used to estimate forces applied to pods.

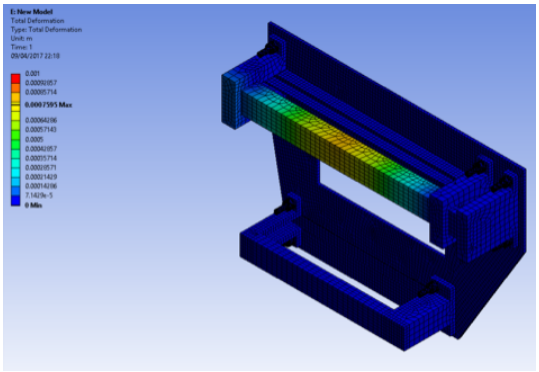

Figure 9: FEA analysis of final frame design.

4.4 CRADLE DESIGN

The design of the cradle was carried out using a combination of experimental and theoretical techniques. The strength of the composite to fastener join was assessed experimentally using servo-mechanical testing. Several different specimens were manufactured with varying composite lay-ups to determine the strength and reliability of the system. Figure 10 shows the experimental set-up for pull-out tests of the Bighead fasteners.

The global strength of the cradle was assessed by creating a free-body diagram of the system to determine the forces and moments applied to the structure. The properties of the laminates used was then determined using a classical laminate theory code, which enabled the stresses within each ply to be calculated. The safety factors applied to the composite cradle were significantly higher than the safety factors applied to the metal frames. This was to represent the increased uncertainty in the strength of the system due to both simplifications in the analysis and the lower confidence in the manufacturing process.

Figure 10: Experimental set-up for pull-out tests of the Bighead fasteners.

4.5 POD SYSTEMS DESIGN

For the Foiling F18 catamaran to be used as a test platform, different settings and positions of the board need to be tested and easily recorded. The three main controls of the board are cant, rake and board height.

4.5.1 RAKE CONTROL

The rake is controlled by a worm drive component, as shown in Figure 12, that moves the top bearing fore and aft. The worm drive is driven by a control line with a take up system under the tramp. The complete model was drawn in SolidWorks to show the maximum and minimum rake angles. Figure 11 shows that the system provides a more than adequate range of rake angles.

4.5.2 UPHAUL AND DOWNHAUL

The main foil is attached to an up and downhaul system to adjust board elevation. Working as a continuous system, the uphaul starts next to the shrouds, in a 4:1 pulley, so one end runs to the top of the mast and back down to the top of the board. The downhaul runs from the metal clamping plate up to the board, back to the bearing frame up to the board and down to another cleat so the board. Figure 13 shows how the up and downhaul system works when the ropes are pulled from the different cleats.

Figure 11: Final Designs rake angles. $A = -8.4°$, $B = 0°$, $C = 13.7°$

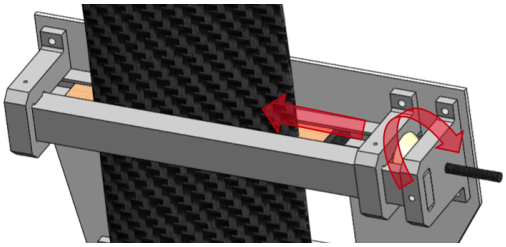

Figure 12: Worm drive system to control the forward and aft position of the foil.

To prevent the foil from being damaged due to being raised too high a preventer line was rigged. This was simply a line running from the pod cradle to the top of the board to stop the board from hitting the hull when fully-raised.

4.5.3 CANT ADJUSTMENT

One of the reasons that the bearings were manufacture out of plywood was for ease of manufacture. This gives scope to laser cut more bearings that can change the angle of cant, due to the tolerances within the frames. These can't be changed during a testing session, but it can provide a good comparison for stability when foiling.

4.5.4 CONCLUSION

A mechanism for attaching lifting foils to a catamaran without the requirement for modifications to the hull has been developed. This has been achieved using a combination of computational tools and experimental testing. The composite cradle has been designed to a safety factor of 4.17 for the pull-through strength of the fasteners attaching the top bearing frame to the cradle and a safety factor of 5.32 for the fasteners in shear. The global strength of the cradle has been designed to have a safety factor of approximately 2 before the failure of $0°$ plys. The metal framing of the pods was also found to have a safety factor of 1.7. The design is considered a success as no structural failings were observed throughout testing (other than a bearing failure), meaning the system requires no modification for future research to take place.

Figure 13: Up and downhaul control system.

4.6 FUTURE WORK

4.6.1 BEARINGS

After multiple tests, it was evident that the bearings had compressed and changed shape. This was problematic when foiling as it allowed the foil to move inside the bearings. These movements caused sudden changes in foil position, leading to changes in the flow around the foils and causing instability when foiling. Ideally, carbon bearings would be used to solve this problem as they are considerably stiffer.

4.6.2 FAIRING

When the boat was successfully tow and sail tested, it was noticeable that the pods were creating a lot of drag. The use of fairing made of a lightweight material, such as CFRP, could significantly reduce drag and take-off velocity, while also covering the hard aluminium frame that could potentially cause injury to the crew.

4.6.3 STRAIN GAUGES

To verify the FEA results, strain gauges can be mounted onto the frame. The strains can be translated into deflection to give a good indication of the forces and deformations of the pods. The strain gauges can be directly linked to the established DAQ system and further used to create a real-time graphical image of stress variations throughout testing. This is an area for future research that can lead to an improved design to either increase strength or save weight.

5 VELOCITY PREDICTION PROGRAM

5.1 NON-FOILING VPP

The non-foiling component of the VPP was essential during the concept design stages of the project to evaluate the non-foiling speeds for each wind angle and direction. Developed

for the F18 in its initial configuration, this program was then compared to data gathered on the water to assess the accuracy. Wind speed data was determined by generating a wind field using data from weather buoys in the vicinity of the testing area. These tests were used to validate the aero component of the VPP, as the rig is to be kept in the same configuration for foiling testing.

5.2 GENERAL METHODOLOGY

Several different approaches were explored for developing a foiling VPP for the platform.

1. Design and code an in house VPP
2. Adapt existing open source VPP
3. Source license to an existing foiling VPP

In order to have a better understanding of how the program works, it was decided to design and write a code from first principles. The program was split up into two main components; a VPP script and the force modules. The idea behind this architecture was to improve the readability of the code by breaking down each area that generates a force into its own module. These modules included sails, foils, aero-drag and mass, with a displacement hull drag module also under development. For a given TWA and TWS, the VPP script generates a first guess, then optimises boat speed until the total force balance of the boat is below a set tolerance. Moment checks are then implemented to ensure pitching and heeling moments are not greater than what can be restored by crew weight [2].

5.3 RIG MODULE

The sail module aims to optimise the maximum forwards force (F_x) to produce the maximum speed at each true wind setting, whilst being constrained by the maximum heeling and pitching moments.

To represent the sailing style of catamarans, the sails are first flattened, to replicate the use of Cunningham, and then sheeting angle increased to replicate easing the traveller. Flattening the sails reduces the total lift, while lowering the centre of effort (Z_{ce}) which decreases the heeling moment further. The sails module loops through sheeting angles and flattening conditions until the moment checks are adhered to and the maximum F_x found [3].

The sail coefficients used are those found in the ORC VPP and were validated during the non-foiling testing of the boat.

When the moment checks are completed, and the best F_x found, the sails module is complete and the resultant forces and moments are outputted for use in the next module. The sail trim for the final solution, sheeting angle and flattening values, are saved for user reference when evaluating each wind condition.

5.4 HYDRO MODULE

The forces generated by the hydrofoils were modelled by assuming the daggerboard was a L-foil canted to an angle θ (As shown in figure 14). This method was employed to allow simple mathematical expressions to be used to determine the lift and drag of the foil. Using a look-up table was considered, however it was deemed that an excessive number of CFD simulations would be required to populate a table with so many variables (i.e. leeway angle, rake angle, depth of immersion, cant, boat-speed).

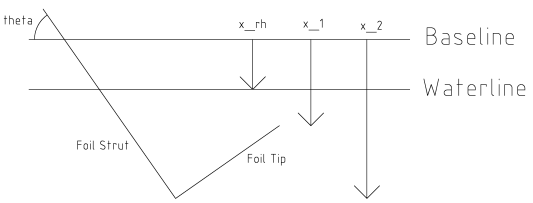

Figure 14: Diagram of simplified foil geometry.

The foil module works by taking the side and vertical force (F_y and F_z) values as inputs, and solves equations 1 and 2 for ride height and leeway angle, at a given boat speed and board rake angle. Values for the area of each section of the foil depend upon ride height (equations 3 and 4), while the lift coefficients of each section of the foil depend on cant, board rake and leeway angle (equations 5 and 6).

$$F_Y = \frac{1}{2}\rho V_S^2(A_S C_{LS} sin\theta - A_T C_{LT} cos\theta) \tag{1}$$

$$F_Z = \frac{1}{2}\rho V_S^2(A_S C_{LS} cos\theta + A_T C_{LT} sin\theta) \tag{2}$$

$$A_V = (1 - \frac{x_{rh}}{x_1})A_{S0} \tag{3}$$

$$A_H = (1 - \frac{x_{rh} - x_2 + |x_{rh} - x_2|}{2(x_1 - x_2)})A_{T0} \tag{4}$$

$$C_{LV} = (1.7\pi(\lambda sin\theta + \alpha cos\theta)) + 0.2 \tag{5}$$

$$C_{LH} = (1.7\pi(\alpha sin\theta - \lambda cos\theta)) + 0.2 \tag{6}$$

The following processes are then undertaken to evaluate the total hydrodynamic drag:

1. The AoA experienced on the strut and tip is calculated from the cant angle, rake angle and leeway angle
2. The C_L is then assumed to be proportional to the AoA.
3. The induced drag of the section is then calculated based on the C_L value
4. Further drag terms such as viscous, wave, spray (and intersection drag for the rudders) are summed to produce total C_D values for the foil and rudders [4]
5. Using the ride-height value, the immersed area of each surface is calculated
6. With the area, drag coefficient and boatspeed known, the total hydrodynamic drag can be assessed

The original VPP, 'VPP1' was a very simplified analysis that failed to take into account the asymmetrical foil section of the hydrofoils. The second iterations of the VPP, 'VPP2' adjusted the relationship between AoA and C_L by providing an intercept i.e. a C_L value at $0°$ AoA. The third iteration, 'VPP3', reduced the proportionality constant from the 2π starting point, based on potential flow theory, to a more modest value of 1.7π. The viscous drag coefficient was also modified to take into account Reynolds number dependency of viscous resistance. These iterations are shown for comparison in Hydrodynamic Validation 5.5.

5.5 HYDRODYNAMIC VALIDATION

CFD analysis was carried out to obtain preliminary data on foil performance, and to provide a comparison against results produced using the VPP. To enable this, the Nacra foils were measured using a Faro gauge to create a geometry file. A rectangular celled structured mesh for the CFD models was generated in Star CCM+ using the Trimmer setting, as it was found to have a good balance between computational time and accuracy [5] [6].

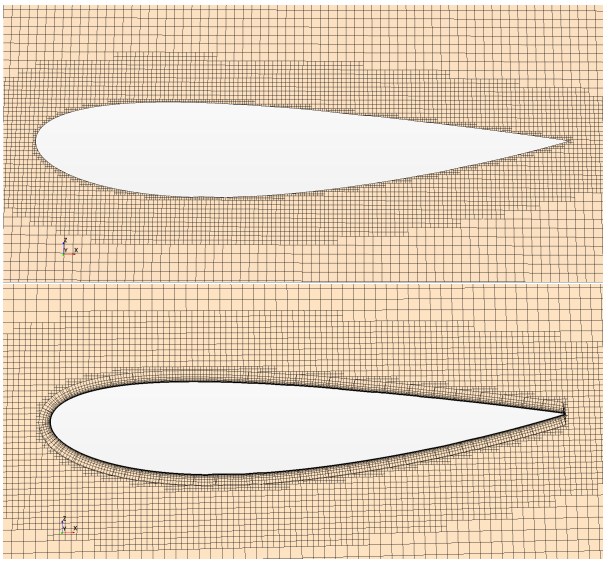

Figure 15: Basis (Mesh 1) and final mesh (Mesh 5) details.

Table 2: Mesh refinement and CFD cases.

Name	Cells
Mesh 1	$6,091,822$
Mesh 2	$7,156,344$
Mesh 3	$27,322,933$
Mesh 4	$1,871,974$
Mesh 5	$11,146,148$

Case	AoA $[°]$	Speed $[ms^{-1}]$
1	4	7.12
2	6	5.66
3	8	4.82

The immersed depth value of the lifting foil was assumed to be $0.85m$. A surface wrapping tool was utilised to generate a continuous mesh (seen in figure 15), and initial runs were carried out using first order upwind schemes to initiate convergence. Convergence with second order schemes was obtained with further mesh adjustments. This was achieved using larger base sizes, no smaller than $40mm$, and minimum target cell sizes of $1.25mm$ on the foil surface. The mesh was further refined to have a properly defined boundary layer, however this proved to be a challenge with regards to computational time and program experience. Four more meshes were generated to carry out a mesh sensitivity study. Mesh sizes and CFD cases are given in Table 2, with the cases chosen based on anticipated speeds and AoA to achieve take-off for the tow tests.

The analysis was set up using the following solvers: steady state, liquid, segregated flow, constant density, turbulent, and K-Omega turbulence models. This was believed to provide an adequate computational representation of the physical flow. The SST K-Omega turbulence model was selected as it is known to be suitable for low speed external aero applications, captures wake better than the K-epsilon model and was found to satisfy y+ conditions and RANS flow [6] [7]. It also has shown to have improved performance for boundary layers [8], and has been found to produce results more in line with experimental tests and lower computational costs [9] [5]. These solvers were found to be successful for the T-foil rudder CFD analysis and produced results that were deemed reasonable. Hence these same solvers were used in the main foil CFD investigation. Appropriate boundary conditions were applied to allow for infinitely large port and starboard walls with a slip condition, and a non-slip condition applied to the foil surface. A custom coordinate system was set up to allow for changes in angle of attack of incoming flow.

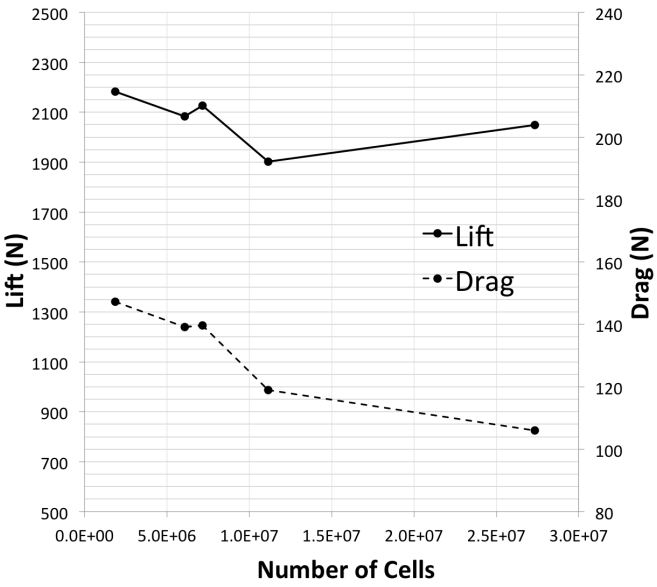

Figure 16: Effect of mesh refinement on lift.

It can be seen from Figure 16 that the lift values obtained from CFD analysis vary within a small percentage with increased mesh refinement for all meshes. A similar trend is seen for drag values except for Mesh 3, in which case the drag was significantly lower. This may be due to sudden changes in cell sizes in the boundary layer and wake areas of the foil. In addition, the computational cost of Mesh 3 was prohibitive and was therefore not considered as a viable option. Mesh 1,

Mesh 2 and Mesh 4 were deemed to have the closest lift and drag values in terms of percentage difference, however it is known that finer meshes with better defined boundary layers are more likely to capture details in the flow, and hence Mesh 5 (seen in figure 15) was chosen to run the cases. It can also be seen that the percentage difference between values for Mesh 5 and 3 were smaller than that of Mesh 2 and 5, supporting this claim. Mesh 5 was found to have a good balance between reliability and computational cost.

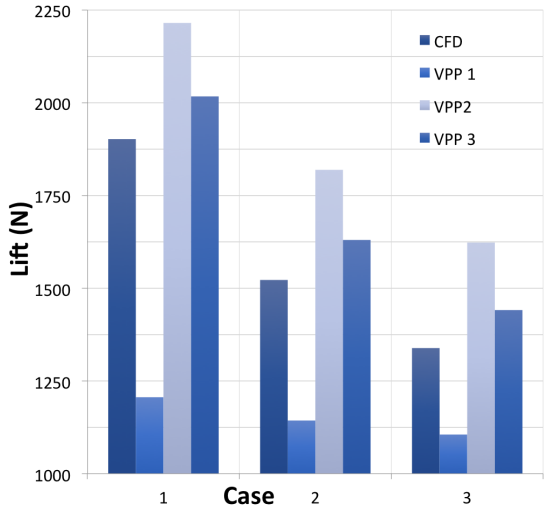

Figure 17: Comparison of CFD and VPP results for lift.

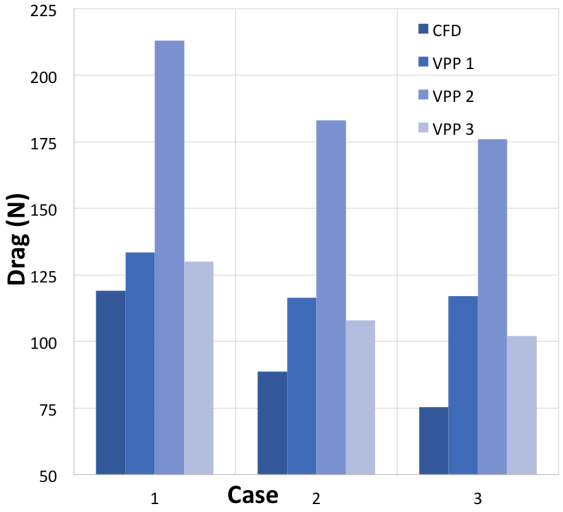

Figure 18: Comparison of CFD and VPP results for drag.

Figures 17 and 18 compare the CFD results to various iterations of the VPP. As the CFD simulations were run without a free-surface, the drag terms due to the foil operating close to the free-surface (wave and spray) were removed from the VPP. VPP 1 generates lift forces considerably lower than the CFD results. This is probably due to not taking the asymmetrical foil section into account. Drag force for this VPP iteration is however quite accurate. VPP mark 2 generates lift forces greater than the CFD results, and drag forces considerably higher. VPP 3 produces both lift and drag forces that more closely resemble the CFD results.

Overall, these results show that there is scope for further investigation for validation of VPP data using CFD, especially for drag forces, as many sources of error exist in both. The largest scope for unreliability in CFD stems from the quality of geometry generated during surface repairs. It was found that the trailing edge had visible imperfections, which was assumed to affect the boundary layer mesh generation. It must be noted that the scanning method of the foils and the geometry manipulation processes used in the computer programs has resulted in the 3D CAD foil model to not completely accurately represent the geometry of the physical foils, but it has provided a good basis for ongoing research and validation of performance prediction. In the future, allowing more time to carry out a more detailed surface repair process could take place in order to provide a more stable surface for further CFD mesh generations. Free surface mesh generation and CFD runs can also take place with a more trustworthy model and mesh, and is an area for further validation and comparison with the velocity prediction program.

6 DATA ACQUISITION

A mobile data acquisition system was designed and constructed to quantify changes and measure the performance of the platform. Further to this, a system to view the data quickly and simply was developed to assess the effects of changes to the platform set-up.

6.1 HARDWARE

In order to get data effectively, data was logged using an android phone, enabling collection of GPS and IMU data. This was combined with a wind field generated by collating data from local weather stations. This method provided enough data to produce the polar plots shown in figure. Despite providing a cheap and reliable system, it was deemed this would not provide enough accuracy for detailed research into the platforms characteristics. It was therefore decided to invest time into the design of a system capable of measuring on board wind and higher frequency GPS data. We decided on a Raspberry Pi due to its low cost, high computing power and large number of GPIO pins, which allows it to be connected to a range of sensors. Further to this, the RPi has built in WiFi allowing remote connection and the potential for live data streaming to remote displays such as smart phones over VNC. After consultation with B&G, it was decided to use a B&G H5000 CPU system in tandem with the RPi.

6.1.1 B&G System

The B&G System compromised of a wind sensor, GPS/Heading Sensor (including heel, trim and yaw angles) and a H5000 CPU to process and filter data. The filtered CPU data was logged instead of the raw data, as this system has been well tested in yacht racing so would not require further post-processing. The RPi was connected to the CPU over ethernet and used the GoFree WebSocket to send data

from the CPU to the RPi using UDP. This is subsequently logged to a text file using WSLogger [10] at around $10Hz$.

6.1.2 IMU & Ultra Sound

The B&G system provided reliable wind and position data, but in order to analyse the hydro-foiling performance, further sensors where required. These consisted of Ultra sound to measure the height of the boat above the water and an IMU to measure the accelerations and rate of turn in 3-axis. The Bosch BNO 055 IMU [11] was used to collect data at $10Hz$.

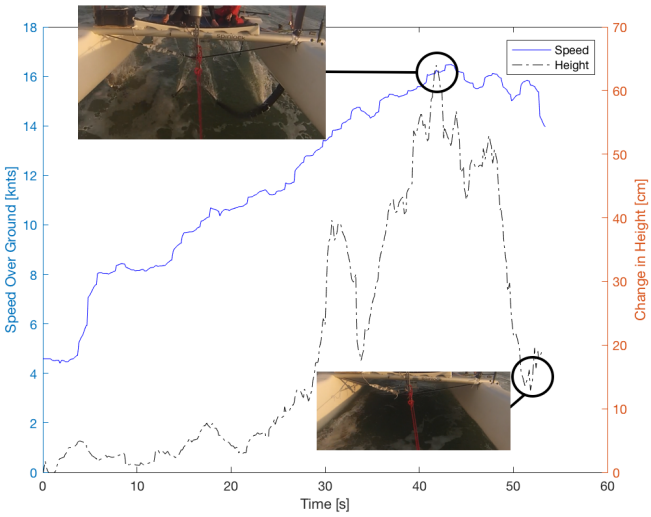

Figure 19: A Take off from tow testing showing the height reading as the vessel takes off and crashes.

Several methods of recording the height of hydro foiling were investigated. Existing systems commonly rely on barometric pressure, with these systems generaly quoting an accuracy of $\approx$ $10cm$ [12], which was not deemed to be of a high enough accuracy for the small changes in elevation that were to be measured. Laser measurement systems are known to have issues on clear water due to the opacity of water, with scatter due to waves also causing innacuracies. Ultrasound provides a solution which works on the surface of water; the HC-SR04 sensor used was tested to have an standard deviation of $1mm$. This system was tested using a CNC translation stage in order to validate accuracy of the sensor. The STANDA translation stage has a stated accuracy of $2\mu m$. Overall the ultrasonic sensor provided a cost effective method for measuring ride height with the HC-SR04 [13]. A lift off from towing testing is shown in figure 19. This shows the ultrasound reading accurately reproducing the height of the platform during the take off, this shows the first take off to occur at $13.5knts$.

6.2 ANALYSIS TOOLS

On the platform there are many metrics being measured at any one time, so to get a full picture of the state of the platform, one must view these in unison. It was decided real time playback would significantly benefit analysis so a data viewer was developed. Initial attempts in Python were very crude and not user friendly, so it was decided to create a webapp. The 'Volanti Viewer' is a javascript based webapp which uses the plotly.js javascript library (a derivative of D3.js) to graph the data, which is loaded in from individual, external, JSON files to reduce the memory usage. This webapp allows for up to 6 metrics to be plotted and played back in sync with each other, as well as scrolling through the data. These features allow the user to analyse the data with a greater understanding of the platforms dynamics.

7 EXPERIMENTAL RESULTS

7.1 STRUCTURAL TESTING

7.1.1 RUDDERS

Throughout testing the rudder performance, during foiling and non-foiling sailing, was analysed. Before testing on the platform could be carried out it was necessary to set the rudders up correctly to maximise performance. An important variable when setting up the rudders is the toe-in angle. By consulting the the Nacra F20 FCS owners manual and through previous experience of sailing catamarans it was decided an angle of toe-in was desirable. The angle of toe-in was set so that the distance between the trailing edges was $2mm$ longer than the measurement at the leading edge. Feedback from the sailors was positive and this set up resulted in rudders that were balanced and not heavily loaded when sailing.

A GoPro camera was fixed on the starboard rudder, allowing observations into the fluid-structure interactions of the T-foils. It can be seen from Figure 20 that the structural strength and length of the rudders, during foiling (whilst being towed), were sufficient to withstand the increased bending moments as immersion was decreased. This was also observed during normal non-foiling and foiling sailing tests. Through these tests, the rudders produced a relatively clean wake individually, seen in Figure 21, but have significant interaction with the wake of the main foil, seen in Figure 20, producing a visible amount of turbulence on the free surface. This did not affect the structural integrity of the components, thus concluding that both the foil design and elevator attachment mechanisms were successful.

Figure 20: Starboard foil and rudder during tow testing.

Figure 21: Starboard rudder during sailing testing.

7.1.2 PODS

Structural testing of the pods was also undertaken using tow testing as due to the lack of side force and a 4-point configuration, the loads were expected to be approximately one third of the load predicted for sailing tests. They were also tested at full load whilst fully sailing. A GoPro camera was positioned just behind the front beam looking backwards at the pods to assess deformations. Images taken with this camera are shown in Figures 22 and 23. The vertical purple lines give an indication of the effect of deformations on the position of the foils during towing and sailing. No damage occurred during testing and the deformations of the structure were deemed acceptable.

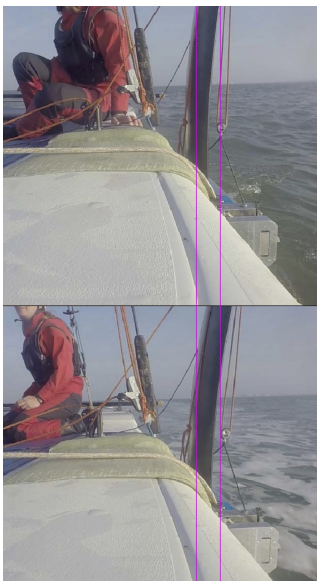

Figure 22: Comparison between position of foil when loaded and unloaded during tow tests

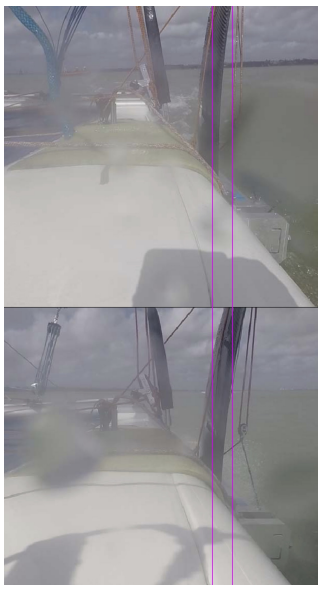

Figure 23: Comparison between position of foil when loaded and unloaded during sailing tests

7.2 TOW TESTING

The first two towing test sessions were undertaken using a RIB limited to $13knots$, however this was still an adequate speed for the platform to foil. Several runs were undertaken varying board rake and elevation to determine the most stable foil configuration. The session proved to be a valuable learning experience, as unforeseen behaviours were observed relating to the propeller wake. The propeller wake is an area of flow with increased velocity and vorticity, which had a large effect on the lift and drag produced by the hydrofoils. It was observed that, even at distances of approximately $20m$ behind the RIB, moving into the wake could cause the lift on the foil to increase dramatically. As such, it was decided that for the next towing session, tests should be carried out with a longer tow line to allow the crew on the platform to steer outside of the wake, making the flow over the foils more representative of normal sailing conditions.

Due to time constraints, a perfect weather window was not available for Test Day Five, so testing was carried out in approximately $10knots$ of wind. Although testing in wind introduced uncertainties due to waves, it also allowed an assessment of the aero drag module to be made by towing the boat in opposite directions and hence different apparent wind angles and speeds. For this session, a more powerful rib was sourced to enable the platform to be tested over a larger speed range. Results were obtained from the DAQ system, with additional drag force data obtained using a Spinlock load cell attached to the tow rope. As the load cell was working at the very bottom of its working range, the drag force was amplified using a 1:2 pulley system. A calibration of this system was carried out to allow for the raw data output from the load cell to be corrected. This corrected value is called 'Corrected Force' in the Table 3.

Table 3: Tow testing results.

Run	Raw Force $[T]$	BSP $[knots]$	Corrected Force $[N]$	AWA $[°]$	AWS $[knots]$	VPP Force $[N]$	% Diff
1	0.07	15.5	495.0	11.8	9.5	551	11.3
2	0.08	16.5	544.1	10.3	8.8	556	2.2
3	0.09	16	590.5	36.6	21.5	721	22.1

The results in Table 3 show that the VPP predicts slightly higher drag force than the measured results. The magnitude of the difference between experimental and measured results is relatively small when it is considered that there is a high degree of uncertainty related to the coarse incremental scale of the load cell. As the hydrodynamic foil section is relatively well validated against CFD data, a potential reason for the over-prediction of drag force could be due to the aerodynamic drag section. A further reason supporting this hypothesis is that the data shows a trend between AWS and percentage difference, with increases in AWS causing an increase in overestimation of drag. As such, further work could look into improving the aerodynamic drag module of the VPP.

The predicted take-off speed and the actual take-off speed were compared to give an indication of the ability of the VPP to predict the vertical force generated by the hydrofoils. This was achieved using speed over ground and ultrasound data recorded from the tow tests. Figure 24 shows a time-series plots of speed over ground (measured using the B&G system) and changes in ride height (measured using the ultrasound sensor) for Run 1. GoPro screenshots of this run found using the DAQ viewer are included at the spikes in ride height to show agreement with physical observations. Figure 19 shows

the same plot for Run 2. These figures generally show a spike in ride height at a given speed, due to the platform lifting out above the water. Both runs shown in these figures were undertaken in the same direction, hence similar tide and apparent wind, and with the same daggerboard rake and elevation settings. Both figures show the first major peak in ride height change occurring at approximately 13.5 knots. Approximately $0.75knots$ of favourable tide was estimated for these runs, making a through the water speed of $12.75knots$. For a board rake angle of $4°$, the VPP predicts a take-off speed of 13.98 knots. There are several factors that could explain the difference between these two results. Firstly, the VPP assumes that the rudders are set at a $0°$ AoA and as such do not produce any lift. However, work carried out in Section 7.2.1 indicates that the rudders may have been generating some degree of lift. Secondly, there is uncertainty related to the exact board rake angle, as this is also strongly influenced by the trim of the boat. Finally, it was observed during testing that aerodynamic lift from the trampoline appeared to have quite a large effect on the dynamics of the platform, potentially causing the earlier than predicted take-off.

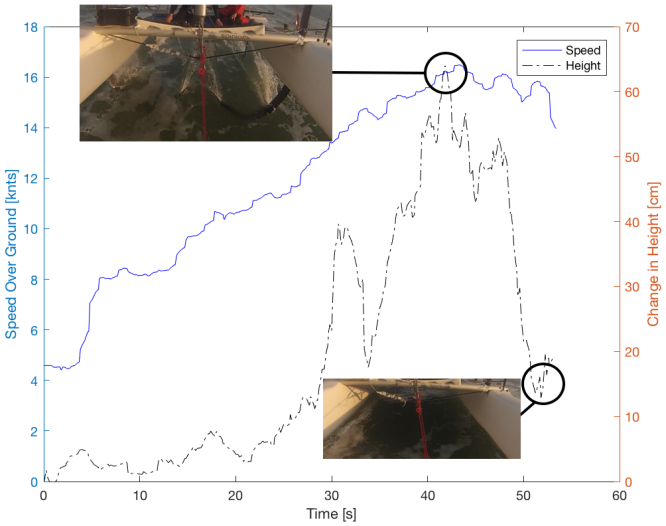

Figure 24: Plot of speed over ground and change in ride height against time for Run 1.

7.2.1 Tow Testing Force Balance

Having achieved stable foiling, a study was carried out to better understand the forces acting on the catamaran. The study was focused on determining the dynamics of the rudder to establish if it was generating positive or negative lift, and the magnitude of this force. A force balance calculation of the boat during a stable section of foiling was carried out.

The DAQ viewer was used to match video data with data collected from the boat to find a stable section of foiling during tow testing. The data from the stable ten second section used for this analysis is seen in Figure 25. Using the load cell, the resistance of the boat can be determined, and therefore it is possible to estimate the foil drag by subtracting the aerodynamic drag. The aero drag of the platform was calculated using the VPP. Using mast head video data the crew position was measured to calculate the LCG of the sailors, with the boat's LCG taken from weights measurements.

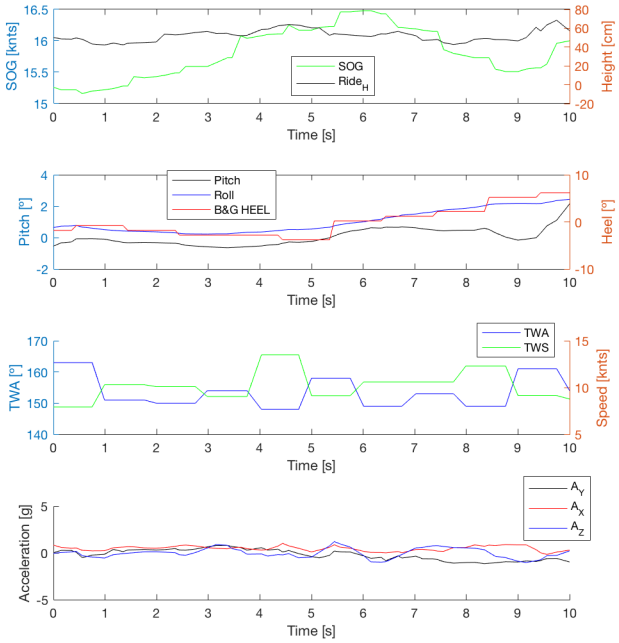

Figure 25: DAQ data during stable foiling.

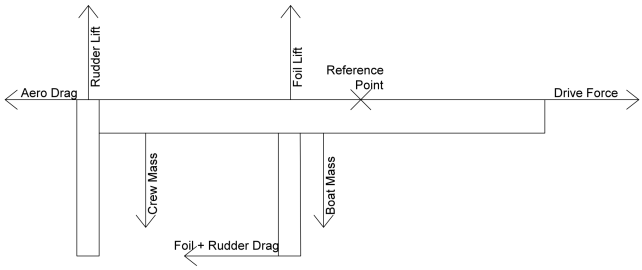

Figure 26: Free-body diagram used for the force balance calculations.

The total lift provided by the foils and rudders was determined using the VPP for the tested boat speed. However, this does not calculate the load distribution between the main foils and rudders. To determine these forces, the free-body diagram in Figure 26 was used to take moments about the mast foot with all of the lift acting initially through the main foil, resulting in an unbalanced equation. To balance this equation the lift provided by the rudder was increased, while main foil lift was decreased, until the moments were balanced. The balanced forces can be seen in Table 4, this shows that the rudders are providing $321.16N$ of lift, or 8% of the total lift.

As a symmetrical foil section was used for the elevator, in order to generate this amount of lift at a boat pitch of $0°$, the rudder set-up on the stern resulted in a pre-set AoA. To cal-

Table 4: Force balance of platform during towing.

AntiClockwise		
Item	Force $[N]$	Position $[m]$
Crew Mass	1373.4	2
Boat Mass	2464.272	0.659
Total Moment	4370.76 $[Nm]$	
Clockwise		
Item	Force $[N]$	Position $[m]$
Foil Lift	3512.85	0.8
Foil & Rudder Drag	469.3	1.27
Rudder Lift	321.16	3
Total Moment	4370.76 $[Nm]$	

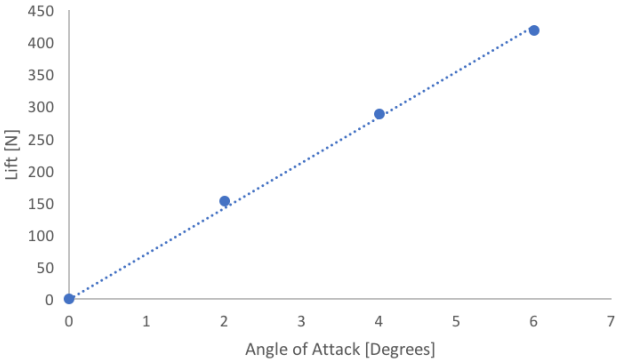

Figure 27: Showing the linear trend of the rudders lift obtained from CFD results.

culate this AoA the rudder CFD data was linearly interpolated, as shown in Figure 27, to find the angle that provideded $160.58N$ of lift at $16.22knots$. The results conclude that the rudders were operating at an AoA of $2.12°$. This equates to a $6.78\ mm$ offset at the top of the rudder.

7.3 FOILING SAILING

7.3.1 Case Studies

Four Point Foiling The first foiling test was carried out in a four-point foiling configuration in attempt to avoid maximum loads for the initial tests. This set-up provides a large amount of lift, therefore relatively low speeds are required for take-off. Figure 28 shows the boat hydrofoiling on all four points. During the review of this test it was noted that the starboard foil was able to pitch, as shown in Figures 28 and 29. This pitching occurred at very low board immersions, with the windward (starboard) board observed in video footage to be pitching forwards, increasing the AoA. This varying AoA of the board with varying foiling height made four point foiling very unstable. The cause of this movement is peculiar as the drag force constantly pushes the foil backwards, so a potential reason is due to tension in the uphaul-downhaul system. The board uphaul pulls the board forwards to the top of the mast, so as the load on the board reduces, tension in the board uphaul could pull the board forwards. Similarly if there is an off-axis component in the downhaul, the system may pull the board forwards as drag force loading is reduced.

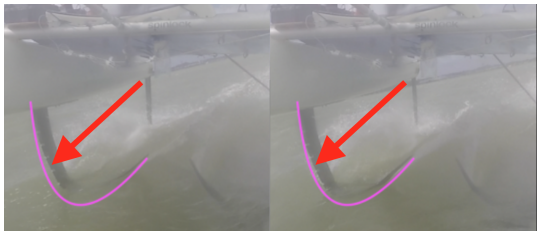

Figure 28: Frontal View of board movement as tip comes out of water during four point foiling.

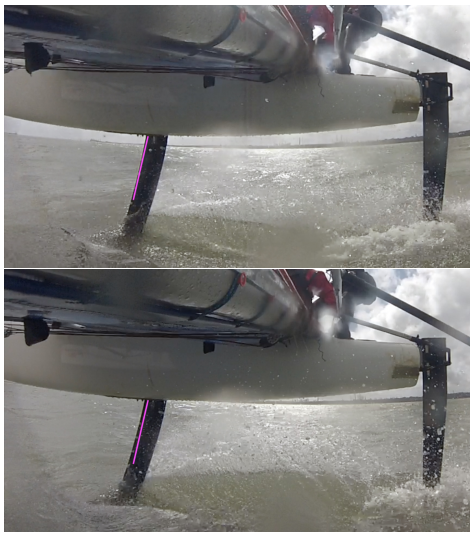

Figure 29: Side view of board movement during four point foiling.

Three Point Foiling Case Study 1 This case study was chosen as the fastest segment recorded on video, showing a duration of steady foiling before violently falling from the foils. Figure 30 shows the data extract obtained for this segment from MATLAB. As the boat accelerates onto the foils, changes in heading can be seen as the boat bears away and heads up to control the power through the varying wind gusts (bearing away to reduce power and heading up to increase it). It can be seen for the first $10s$ these changes are small and subsequently changes to power remain small, at $10s$ at the change in heading is large and sharp as shown by the rate of turn. This caused a rapid increase in power, increasing the lift on the board causing the boat to rise too high too quickly, expose the foil tips reducing lift and subsequently drop back into the water. This is shown by the drop in acceleration in the z-axis, causing a rapid deceleration at $12.5s$ as shown in the X acceleration change immediately after. This highlights the need for small and smooth changes in heading, and the difficulty in sailing gusty conditions.

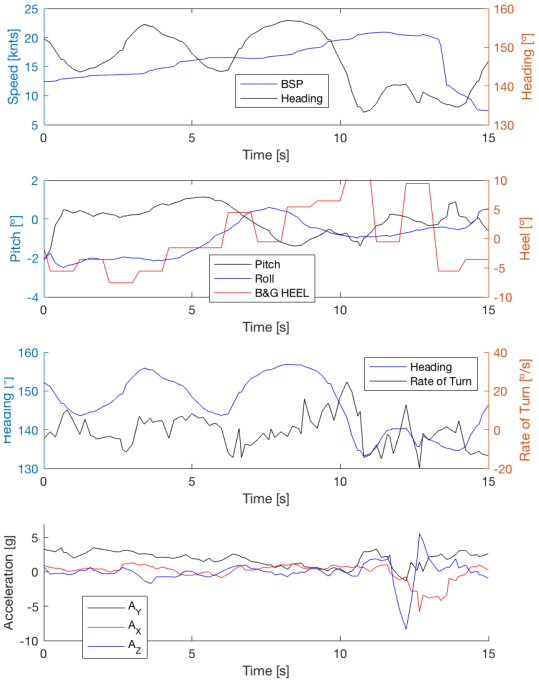

Figure 30: Speed, heading, rate of turn and accelerations corresponding to the times in Figures 31, 32 and 33.

Figure 32: Heading up to power boat back up. $T = 12.5s$.

Figure 31: Bearing away de-powering the boat. $T = 11s$.

Figure 33: Crashing back into the water. $T = 14s$.

Three Point Foiling Case Study 2 Cant is an incredibly important variable in the stability of foiling. The relatively low cant of our platform can be seen to have adverse effects on the stability as shown in Figure 34. This shows stable foiling for the first $10s$, however during this period the heel is reducing as shown in the second plot. This is also observed in the visible change in heel between images at $6s$ and $10s$, with the images at $6s$ shows the tip piercing the water, controlling the heave of the vessel. As the boat comes flat from $6 - 10s$, the cant of the board is effectively reduced which in turn reduces the heave stability of the platform. Just after $10s$, $5°$ of windward heel is observed. The boat lifts further out of the water, as shown by the spike in vertical acceleration, and subsequently crashes. This indicates that in order to achieve stable flight, the effective cant of the daggerboards should be increased.

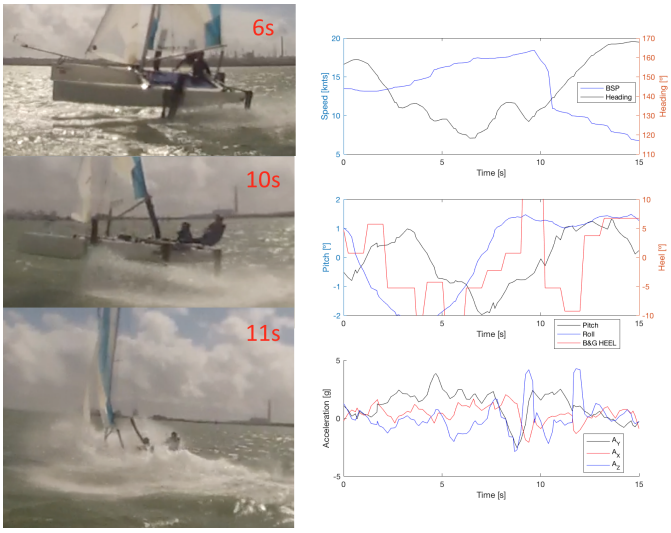

Figure 34: Plots of data and images showing a crash from foiling caused by lack of cant.

7.3.2 VPP Comparison

Figure 35 shows a polar plot of raw data, filtered data and predicted speeds. The filter applies an average to the fastest four data points within a six degree TWA angle. The data shows top speeds were recorded on starboard tack. This was due to damage occurring to the lower board bearing on the starboard side, which reduced the foil rake of this board, preventing the boat from foiling on port tack. The results of Figure 35 show that the VPP predicts considerably higher boat-speeds than those obtained during testing (for TWA $< 140°$). However, this sailing session was the first time some of the crew had sailed hydrofoiling boats, so the boat would not have been sailed to its full potential. The VPP is also a steady-state idealised prediction, so doesn't take into account variations in wind and sea-state. The results show anomalous speeds in excess of the predictions for TWA $> 140°$, however, as can be seen from the raw data, these were not equilibrium conditions and therefore not predicted by the VPP. Feedback from the sailors suggested that these values where only obtained during bearing away in gusts when foiling, and thus would not be achievable in steady-state sailing.

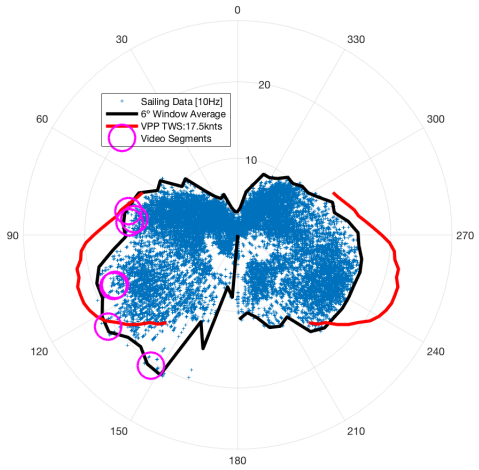

Figure 35: Comparison of VPP data with the raw testing data, averaged sailing data and steady foiling segments highlighted from video footage.

7.4 VPP Evaluation

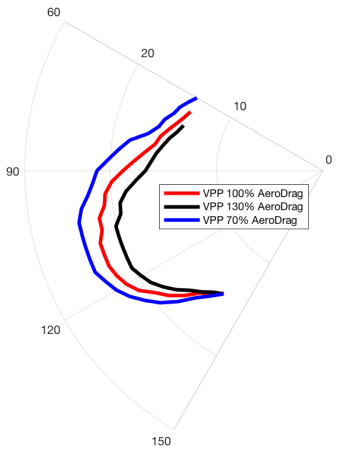

Figure 36: Effect of aerodynamic drag on polars for $TWS = 17.5knots$.

While the hydrodynamic and sails VPP modules have been validated to an extent, the aerodynamic drag is based on empirical data. As such, it is possible that aerodynamic drag is underestimated. The effect of the aerodynamic drag on the VPPs predictions are shown in Figure 36, this shows that the aerodynamic drag has a large effect on the predicted speeds; increasing the aerodynamic drag decreases the predicted speeds. It is recommended that more research is conducted into the validation of the aerodynamic drag forces as these are seen to have significant influence on the results obtained from the VPP.

The VPP indicated that, other than for TWA $< 80°$, pitching moment limits were reached proving to be a limiting factor on boat speed. This was also observed during the testing

session, as the crew were positioned as far aft as possible for all foiling runs. Feedback from the crew also indicated that they felt capable of holding more power in heel, but were constrained by the pitching moment.

The VPP results also show that as TWA is increased from $120°$ to $150°$, boat speed drops significantly due to large changes in AWS and AWA. This makes two-sail broad-reaching a challenge, as the upwind sailset efficiency of the main and jib reduce rapidly at these wind angles. The addition of a spinnaker may help in reducing this rapid change in drive force with course angle.

Figure 37 investigates the change in crew weight, showing that for a TWS of 17.5 knots, reducing crew weight increases predicted boat speed for TWA $< 80°$ and decreases boat speed above these wind angles. This follows conventional wisdom that extra crew weight helps provide more righting moment, improving performance upwind, while increasing resistance due to greater foil AoAs required downwind.

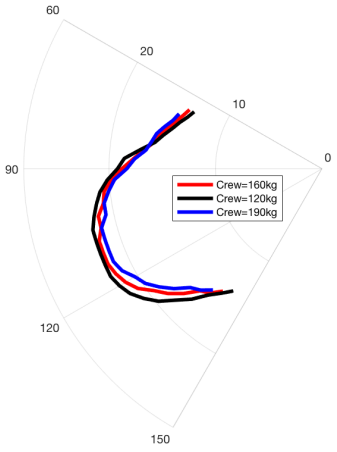

Figure 37: Effect of crew weight on polars for TWS $= 17.5knots$.

A study was carried out to assess the effect of crew weight over a larger wind range, with Figures 38 and 39 showing predicted speeds for varying crew weights at a TWS of $13.6knots$ and $21.4knots$ respectively. These figures show that in the lighter winds a lower crew weight increases the range of TWA for which the platform can foil, with a crew weight of $190kg$ proving too heavy for take-off in a TWS of $13.6knots$. In heavier winds, the range of TWAs for which heavy crew weight has a performance advantage is increased, with the heavier crew of $190kg$ having an advantage up to TWAs of approximately $110°$.

Figure 40 explores the effect of board rake angle on the predicted speeds. As expected, the highest boat speeds were achieved with lower rake angles, due to the reduced induced resistance. However, the reductions in rake angle also reduces the range of wind angles that the platform is capable of foiling in. A crossover between optimum rake angle is also observed between TWAs of approximately $110 - 120°$. This could be explained by the lower board rake angles requiring a greater immersion to provide the required lift, hence increased drag.

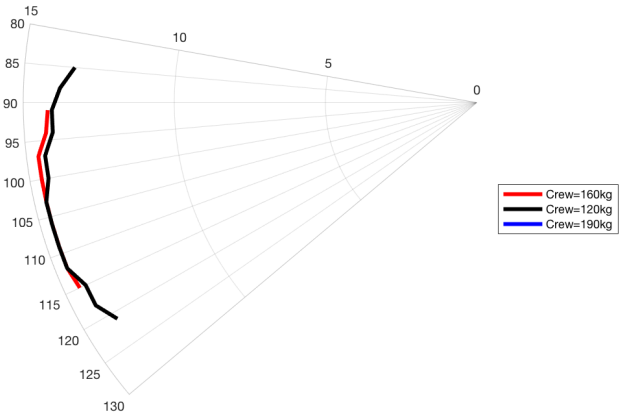

Figure 38: Effect of crew weight on polars for TWS $= 13.6knots$.

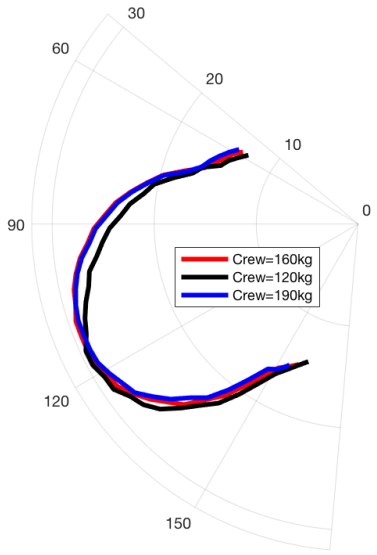

Figure 39: Effect of crew weight on polars for TWS $= 21.4knots$.

This shows that optimum board rake angle is not just simply the minimum possible rake required to foil; the most efficient set-up has to minimise both induced drag and immersed area.

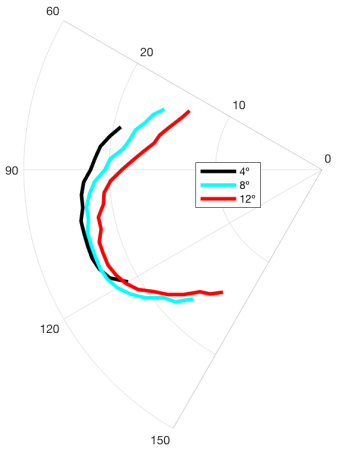

Figure 40: Effect of board rake angle on polars for TWS $= 17.5knots$.

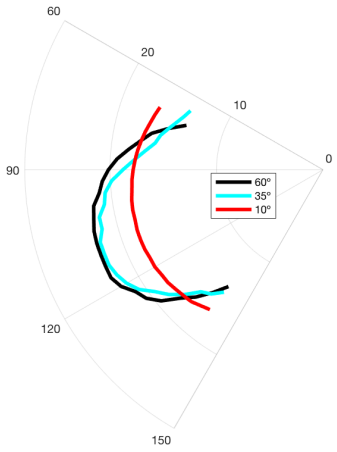

Figure 41: Effect of board cant for TWS $= 17.5knots$.

As previously discussed, cant has a large influence on the stability of the platform, however it also has an impact on the performance. Figure 41 is a particularly interesting plot showing predicted boatspeeds for a range of cant angles. The plot shows that at very low and very high TWAs, reducing cant improves performance, while at reaching angles between approximately $90 - 130°$, reducing cant has a detrimental effect on performance. This is a surprise, as generally decreased cant is considered to be fast and unstable, while increased cant is considered slower but more stable. A potential reason for the VPP polar plot disagreeing with this is that tips of the lifting foils could be too small for the platform, as the platform is considerably heavier than the Nacra F20 FCS that the foils were designed for. This could mean that at low cant angles, a large degree of board immersion is required to achieve take-off, increasing foil drag. By increasing cant, the daggerboard strut contributes more to the vertical lift, reducing the required immersed foil area and hence drag. Two further causes for this strange behaviour could be due to limitations in the VPP code. The VPP does not take into account reduction in righting moment due to increasing cant, which would limit the amount of drive force the boat was capable of applying while staying within the righting moment checks. The code also does not currently loop through board rake angles to find the optimum; instead board rake angle is a user-defined input.

8 CONCLUSIONS

A test platform has been developed to allow a F18 catamaran to foil without the need for any hull modifications. This entailed the design and manufacture of a foil attachment system and T-foil rudders. The design methodology involved a variety of analytical, computational and experimental methods within a short time frame, all while considering strict budget constraints for manufacture. The systems have been tested in strong wind conditions and proved to be robust and structurally reliable.

The DAQ has proved to be a reliable system for recording the platform metrics. The system has allowed for video footage to be compared with quantitative data to improve understanding of the performance and behaviour of the platform. The system is also not bespoke for a foiling catamaran; the standalone nature means it can easily be removed and used to gather data for other sailing related research projects.

A foiling VPP suitable for modelling L-foils has been developed and compared to both numerical simulations and on the water data. Different components of the VPP have been assessed separately. The sails module successfully predicted the non-foiling boat performance and the hydrodynamic module foil drag predictions are very close to the results from the CFD. Using the VPP the take-off speed of the platform was accurately predict and validated by the ultrasound results from tow tests.

The combination of the foiling platform, DAQ and VPP will allow future research into foiling technologies.

9 ACKNOWLEDGEMENTS

The authors would like to thank B&G for the loan of the H5000 CPU and wind sensor, BigHead for supplying the fasteners used in the testing and construction of the foil attachment system, Spinlock for the loan of a LD Sense load cell, Land Rover BAR for supplying pre-preg carbon fibre, and Green Marine for the use of their facilities and expertise in the manufacture of the rudders.

REFERENCES

[1] ISAF, *INTERNATIONAL FORMULA 18 CATAMARAN CLASS RULES*, 2016 (accessed January 3, 2017). http://www.sailing.org/tools/documents/F182016CR010316-[20541].pdf.

[2] M. W. Findlay and S. R. Turnock, "Investigating sailing styles and boat set-up on the performance of a hydrofoiling Moth dinghy," *20th International HISWA Symposium on Yacht Design and Yacht Construction*, 2008.

[3] A. Claughton, F. Fossati, D. Battistin, and S. Muggiasca, "CHANGES AND DEVELOPMENT TO SAIL AERODYNAMICS IN THE ORC INTERNATIONAL HANDICAP RULE," *20th International HISWA Symposium on Yacht Design and Yacht Construction*, 2008.

[4] HOERNER SIGHARD .F., *Fluid-Dynamic Drag*. HOERNER FLUID DYNAMICS, 1965.

[5] K. Ren, J. Hu, X. Xiong, L. Zhang, and J. Wei, "Validation of Turbulence Models in STAR-CCM+ by N.A.C.A. 23012 Airfoil Characteristics," no. January, 2009.

[6] CD-Adapco, *STAR-CCM+ Reference Guide*. 2012.

[7] J. Banks, L. M. Giovannetti, S. R. Turnock, and S. W. Boyd, "Developing tools for assessing bend-twist coupled foils," pp. 1–6, 2014.

[8] F. R. Menter, "Two-equation Eddy-Viscosity Turbulence Models for Engineering Applications," *AIAA J.*, vol. 32, no. 8, pp. 1598–1605, 1994.

[9] W. D. Mackenzie, Alasdair, Alejandro Lopez, Konstantinos Ritos, Matthew Stickland, "A Comparison of CFD Software Packages' Ability to Model a Submerged Jet," in *Elev. Int. Conf. CFD Miner. Process Ind. CSIRO*, no. December, pp. 1–4, 2015.

[10] A. Bryson, *WSLogger*, 2014 (accessed January 3, 2017). https://github.com/AndyBryson/WsLogger.

[11] Bosch, *Bosch BNO055*, (accessed January 10, 2017). https://www.bosch-sensortec.com/.

[12] Farnell, *MS5637-02BA03 Pressure Sensor*, (accessed December 14, 2016). http://uk.farnell.com/measurement-specialties/.

[13] CPC, *MULTICOMP HC-SR04 ULTRASONIC DISTANCE SENSOR*, (accessed January 10, 2017). http://cpc.farnell.com/.